Investigating changes in transport, kinetics and heat generation over NCA/Gr-SiOx battery lifetime

Malgorzata E. Wojtala[1], Ferran Brosa Planella[2,3], Alana A. Zulke[3,4], Harry E. Hoster[3,4,5], David A. Howey[1,3*]
[1]*Department of Engineering Science, University of Oxford, Oxford, OX1 3PJ, UK*
[2]*WMG, University of Warwick, Coventry, CV4 7AL, UK*
[3]*The Faraday Institution, Harwell Campus, Didcot, OX11 0RA, UK*
[4]*Department of Engineering, Lancaster University, Lancaster, LA1 4YB, UK*
[5]*The Hydrogen and Fuel Cell Center ZBT GmbH, Duisburg, 47057 Duisburg, Germany*

Corresponding author: david.howey@eng.ox.ac.uk

***Abstract*—We present a study of battery ageing, comparing pristine, calendar-aged, and cycle-aged lithium-ion cells. Insight into degradation was obtained via differential voltage analysis and by estimating and tracking changes in a subset of electrochemical model parameters of the single particle model through inverse modelling. We show that both diffusion time and kinetic overpotential increase in cycle-aged cells, while calendar-aged cells experienced no diffusion time changes but some kinetic overpotential increase. The latter is also evident in 50% higher irreversible heat generation in cycle-aged cells. This study highlights the importance of updating battery model parameters during ageing.**

***Index Terms*—battery, degradation, diffusion, heat**

I. Introduction

The accelerating transition towards electric vehicles (EVs) in the automotive industry motivates further research into design and optimisation of energy storage solutions, where an ongoing challenge is understanding and predicting battery degradation. The current inaccuracies of predictive models and state observers means that an average Li-ion battery may not be used at its full capability [1]. Uncertainties increase as a battery ages, because most predictive models use parameters obtained from a brand new cell. Additionally, aged cells may experience increased heat generation leading to safety concerns and higher cooling system energy consumption.

Electrochemical models offer a good approximation of the physical processes occurring within a battery, such as electrode and electrolyte mass- and charge-conservation, energy conservation, and reaction kinetics [2]. Through careful tear-down procedures (e.g. half cell construction), electrochemical model parameters may be estimated. However, reparameterisation of model parameters as a battery ages is almost impossible in commercial cells, because half cell potentials change with respect to one another and batteries do not typically contain reference electrodes.

This research was funded in whole or in part by The Faraday Institution "Multi-Scale Modelling" project [EP/S003053/1, grant numbers FIRG003 and FIRG025] and by an EPSRC Industrial CASE Award.

This work presents a comparative ageing study of changes in a subset of parameters of an electrochemical model of a Samsung 35E nickel-cobalt-aluminium (NCA) 18650 cell with graphite-silicon (Gr/Si) anode. The goal of the study is to identify the main degradation modes that occur and to track transport and kinetics changes throughout lifetime by adjusting model parameters. To estimate parameters, a single particle model (SPM) was simulated in COMSOL and parameters were updated with Matlab LiveLink. We conclude that the parameters impacted by ageing include diffusion time, stoichiometry, active material volume fraction and kinetic rate constant. The impact of this work is two-fold. Firstly, we highlight how the SPM can be used to accurately simulate both pristine and aged cell voltage responses if model parameters are updated accordingly. From a battery management system perspective, this ensures accurate state of charge, power etc. estimation throughout life, and maximum use of available capacity. Secondly, this study provides qualitative insight into the impact of ageing on model parameters, which may inform safety issues such as increased heat generation.

II. Experimental

Three batches of Samsung 35E NCA/Gr-Si (90% wt Gr, 10% wt Si) cells with 3.4 Ah nominal capacity were subjected to different degradation scenarios. The first batch, consisting of three cells, experienced one year of calendar ageing at 75% state of charge (SoC) and 45 °C, which resulted in 7.6% capacity loss. The second batch, also consisting of three cells, experienced continuous cycling with 2 A constant current charging until 4.2 V and 2 A constant current discharge until 2.5 V at 45 °C [3], and after 720 cycles had lost 21.5% of its initial capacity.

Before and after ageing, all groups were subjected to nondestructive characterisation tests to enable model parameterisation. A C/20 constant current (CC) discharge was used to calculate cell capacity. This was followed by a galvanostatic intermittent titration test (GITT) consisting of 600 s, C/10 current pulses with 2 h rest periods. Upon completion of the ageing protocol, one cell from each group was chosen as representative for that group and used for the model

Parameter	Description	Ψ_+	Ψ_-	Method
	Parameters that are assumed constant throughout life			
L	Coating thickness (μm)	71.5	83.3	Measured (per side)
A	Electrode active area (m^2)	0.036285	0.036285	Measured
R_p	Mean particle radius (μm)	1.2	1	Measured
α	Charge transfer coefficient ($-$)	0.5	0.5	Assumed
$c^{\max}$	Maximum concentration of Li in solid material ($\mathrm{mol}/\mathrm{m}^3$)	48000	31398	Theoretical/estimated
	Initial values of parameters subsequently tracked with ageing			
D	Diffusion coefficient (m^2/s)	1.9e-16	function	Estimated from GITT
x	Stoichiometry at 100% SoC ($-$)	0.26	0.74	Estimated
ε_s	Active material volume fraction ($-$)	0.8	0.875	Measured
k	Kinetic rate constant (m/s)	5.5e-11	5.5e-11	Optimised

TABLE I: Summary of pristine cell parameter estimates; Ψ_+ and Ψ_- are positive and negative electrode parameters respectively.

parameterisation and heat study. An Artemis motorway drive cycle scaled for maximum 1C current was used for model parameter estimation, while 1C and C/3 CC discharge tests were used for the heat generation study.

The experiments were conducted using a Maccor 4200 series battery cycler, with temperature measured on the surface of each cell with T-type thermocouples ($\pm 0.5\,^\circ$C, RS Pro). The thermocouples were calibrated against an Omega P-M series RTD (class A) in a thermal bath (Julabo 900 F). For temperature stability, all cells were placed in a thermal chamber set for 20 °C. To avoid forced and uneven convection the thermal chamber fan was switched off throughout duration of all tests except the GITT. Additionally, battery tear-down and a set of standardised parameterisation procedures described in [4] were performed to obtain additional electrochemical parameters required for the model. All resulting model parameters for a pristine cell are summarised in Table I.

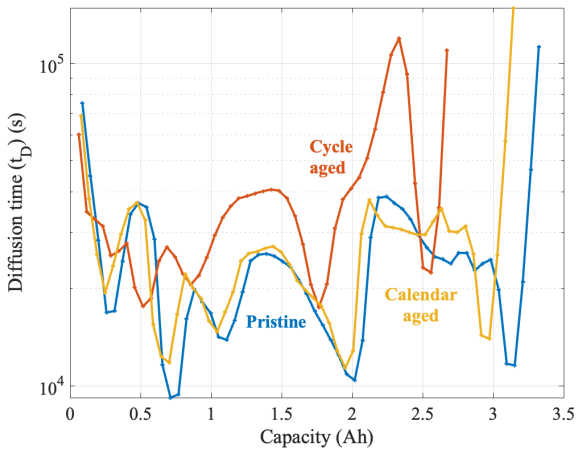

Fig. 1: Full cell diffusion time (t_D) comparison for pristine, calendar aged and cycle aged cells.

III. Electrochemical model

The SPM assumes that all particles within each electrode behave identically and hence they can be modelled by a single representative spherical particle. Additionally, the reaction current is assumed to be uniform in the through-plane direction across the porous electrodes, and the potential gradients within the electrodes are neglected. The local potential and concentration gradients within the electrolyte are ignored and accounted for using a lumped solution resistance term [5]. The SPM assumes that the electrolyte effects are negligible, which is correct for relatively low C-rates. More details on the SPM can be found in the literature [2] [6].

A. Diffusion time

Conventionally, diffusion is characterised by the Fickian diffusion time scale, which is extracted from GITT, potentiostatic intermittent titration tests or electrochemical impedance spectroscopy measurements. Alternative approaches involve Bayesian estimation [7], and direct model fitting to the experimental data [8]. In this work, Sand's approach [9] was used to extract the diffusion time $t_{D_\pm}$ from GITT data, according to

$$\frac{1}{t_{D_\pm}} = \left(\frac{D_\pm}{R_\pm^2}\right) = \frac{4}{\pi}\left(\frac{I}{3FA_\pm L_\pm}\frac{\mathrm{d}E_{\mathrm{OCP}\pm}/\mathrm{d}c_\pm}{\mathrm{d}E_\pm/\mathrm{d}\sqrt{t}}\right)^2, \quad (1)$$

where $D_\pm$ is diffusion coefficient, $R_\pm$ is effective particle radius, $A_\pm$ is electrode plate area, $L_\pm$ is the electrode thickness, F is Faraday constant, $E_{\mathrm{OCP}\pm}$ is open circuit potential, $c_\pm$ is lithium concentration, I is applied current, $E_\pm$ is the measured voltage and t is time.

The estimated diffusion time as a function of state of charge for a full cell is plotted in Fig. 1 for pristine, calendar and cycle aged cells. The calendar-aged diffusion time profile has very similar magnitude and shape to the pristine cell, but squeezed in the capacity axis, due to electrode balancing changes (confirmed with DVA). In contrast, for the cycled aged group there is both a horizontal compression and a large increase in magnitude of diffusion time, reflecting longer relaxation times that could be caused by changes to diffusivity

or effective particle radius or both. This shows that diffusion time is an important ageing parameter, although it is often assumed constant in the literature [2] [10] [11]. Additionally, Fig. 1 reveals a strong dependency of diffusion time on SoC. Note that the method used for estimating diffusion time may be affected by large overpotentials that dominate at the beginning and end of the discharge voltage profile, and consequently, visible extremes close to $0\,\mathrm{Ah}$ and $3.4\,\mathrm{Ah}$ may not be representative.

An estimate of the effective diffusion coefficient can be made from the diffusion time by assuming an effective particle radius, which we took to be the radius of graphite particles since the composition of the anode is mostly graphite. The effects of the characteristic volume expansion/contraction of silicon [12], although not included in the SPM particle definition (assumed constant), are reflected in the measured OCP of the anode.

The MATLAB curve fitting toolbox is used to define diffusion time as a function of anode lithiation. The resultant function is then used as a direct input to the model. Given the observed increase in diffusion time for cycle-aged cells, an additional diffusion ageing parameter, $\lambda_{D\_}$, is introduced. The $\lambda_{D\_}$ premultiplies the D_- term in the model and effectively, any change in diffusivity, particle size or both caused by ageing is expected to manifest in $\lambda_{D\_}$ change.

B. Selection of parameters to track during ageing

To choose the most appropriate parameter subset for tracking during ageing, an initial quantification of the degradation modes experienced by each group of cells was conducted using differential voltage analysis (DVA) [3]. The resulting DVA ageing markers are shown in Fig. 2. In case of calendar-aged cells, the capacity fade $\mathrm{Q_{full}}$ seems to be caused mostly by loss of lithium inventory (LLI) [13], which manifests in electrode balancing changes $\mathrm{Q_{LLI\ balance}}$ that shift the stoichiometry of the cell $x_\pm$. Based on Fig. 1, the diffusion time λ_D has not significantly changed during calendar ageing. The kinetic rate is assumed constant with SoC, and equal in both anode and cathode—it is expected to change with calendar ageing at elevated temperatures due to SEI side reactions. Therefore, the *tracked ageing parameters* for calendar aged cell were selected to be the stoichiometry at 100 % SoC x_+ and x_- and the kinetic reaction rate constant k_-.

In contrast, for the cycled group of cells in Fig. 2 we observe a substantial decrease in anode capacity $\mathrm{Q_{LAM,NE}}$, resulting from loss of the active material (LAM) [14] which decreases the accessible area on the electrode. Since A_- and $\varepsilon_{s,-}$ are linked geometrically (for a constant effective particle radius), according to

$$A_\pm = \frac{3\varepsilon_{\mathrm{s},\pm}}{R_\pm}, \tag{2}$$

we therefore assume that only $\varepsilon_{s,-}$ changes.

The reason for loss of active material is not identified, but one explanation involves changes in the particle size [15]. Interestingly, Fig. 1 shows a substantial magnitude change in the diffusion time for the cycle-aged cells—this could be influenced by particle morphology changes. The specific reason cannot be unequivocally identified, but $\lambda_{D\_}$ is expected to change. Additionally, an electrode balancing shift $\mathrm{Q_{LLI\ balance}}$ is observed, therefore changes in x_+ and x_- are expected for the cycle-aged cells. Fig. 2 also shows a decrease in cathode capacity $\mathrm{Q_{LAM,PE}}$, however both electrode parameters cannot be simultaneously fitted uniquely, and therefore henceforth we assume that only the anode parameters are changing, and we hold the cathode parameters constant. In summary, the *tracked ageing parameters* for the cycle-aged cells are the diffusion correction factor λ_D, stoichiometries at 100% SoC x_+ and x_-, kinetic reaction rate constant k_-, and active material volume fraction $\epsilon_{\mathrm{s},-}$.

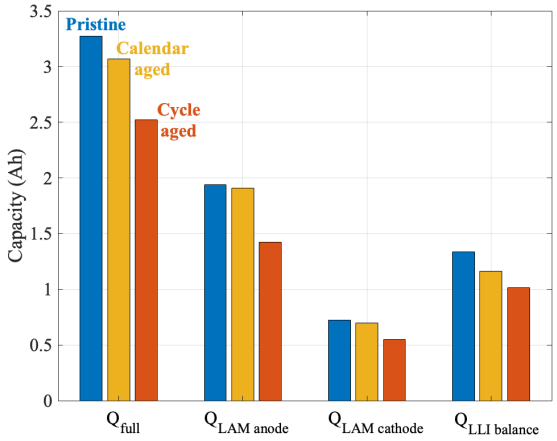

Fig. 2: Ageing markers extracted from DVA of charge data for pristine cells at beginning of life, plus calendar- and cycle-aged cells at end of life. The evolution of these ageing markers across all reference performance tests is available in our previous work [3].

C. Parameter estimation

To track the subset of ageing parameters discussed in the previous section, we minimised the cost function given by (3)—this is a standard least-squares minimisation problem solved with MATLAB `lsqnonlin`, aiming to identify the parameters that give the optimal fit between model simulated and experimentally measured battery voltage. The optimisation problem can be written as

$$\begin{aligned} \min_\theta \sum_{i=1}^{N} \left(E_i^{\mathrm{sim}} - E_i^{\mathrm{exp}}\right)^2, \\ \theta = \{\theta_1, \theta_2, \ldots \theta_n\}, \\ \theta_k^l \leqslant \theta_k \leqslant \theta_k^u, \end{aligned} \tag{3}$$

where the superscripts sim and exp represent simulation and experimental measurements. The index i corresponds to the entries in time t of the experimental and simulated voltages, and N is the number of measurement points i for each experiment. Parameters were constrained between upper and

lower bounds. For each group of cells, the optimised parameter sets are

$$\theta_{\text{pristine}} = \{x_+, x_-, k_-, \lambda_{D\_}\}, \tag{4a}$$
$$\theta_{\text{calendar}} = \{x_+, x_-, k_-\}, \tag{4b}$$
$$\theta_{\text{cycle}} = \{x_+, x_-, k_-, \varepsilon_{\text{s}-}, \lambda_{D\_}\}. \tag{4c}$$

The remaining parameters for the calendar-aged and cycled cell models were assumed constant, and set to the optimised values found for a pristine cell.

D. Sensitivity analysis

Sensitivity analysis was used to explore the local identifiability of parameters. Each parameter was subjected to a small magnitude change, $\Delta\theta$, and the associated output change S_i was recorded (in this case S_i is a row vector of voltages versus time, reflecting the impact of the parameter change on the measured output throughout the drive cycle). The $\Delta\theta$ used here was 1e-8 $*$ θ_i, where θ_i corresponds to a nominal value of the parameter vector

$$\theta_i = [x_+, x_-, k_-, \varepsilon_{\text{s}-}, \lambda_{D\_}]^T. \tag{5}$$

Each parameter θ_i was perturbed one-at-a-time and the corresponding S_i vectors calculated, then stacked, creating matrix $S = [S_1, S_2, S_3, S_4, S_5]$ [16]. Then a pairwise linear correlation coefficient was calculated between each pair of rows in the matrix S [16]. By the Cauchy-Schwarz inequality

$$-1 \leq \frac{\langle S_i, S_j \rangle}{\parallel S_i \parallel \parallel S_j \parallel} \leq 1. \tag{6}$$

The closer the correlation coefficient to zero, the more orthogonal the parameters and hence the more uniquely identifiable they are [16].

Given that the non-constant current profile improves identifiability, pristine cell was simulated over an Artemis motorway drive cycle and the correlations calculated. The resultant correlation matrix C is

$$C = \begin{bmatrix} 1 & . & . & . & . \\ 0.46 & 1 & . & . & . \\ 0.34 & 0.41 & 1 & . & . \\ 0.40 & 0.45 & 0.31 & 1 & . \\ 0.34 & 0.46 & 0.57 & 0.35 & 1 \end{bmatrix}. \tag{7}$$

The sensitivity values oscillate around 0.31-0.57, which means that for all parameters a unique optimal value can be found and model can be successfully simulated.

E. Heat-balance

To understand the implications of the ageing results for battery thermal management, a reversible heat Q_{rev} and irreversible heat Q_{irr} (9) are simulated using the data from each group of cells.

The reversible heat (8), related to the entropy change, is defined by partial change in the open circuit potential E_{OCP} with respect to temperature T at constant pressure p and state of charge x. This is taken from our previous work [3].

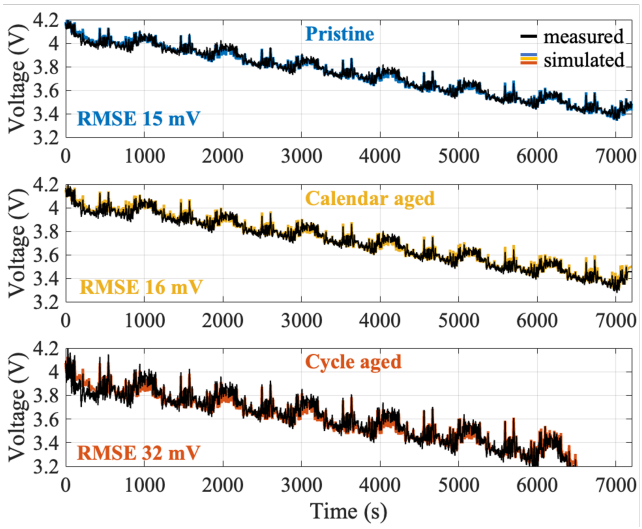

Fig. 3: Artemis motorway drive cycle voltage simulation results for pristine, calendar-aged and cycled-aged cells.

$$Q_{\text{rev}} = IT\left(\frac{\partial E_{\text{OCP}}(x,T)}{\partial T}\right)_{p,x} \tag{8}$$

The irreversible heat source term is the difference between the E_{OCP} and an output voltage E multiplied by applied current I.

$$Q_{\text{irr}} = I\left(E - E_{\text{OCP}}(x,T)\right) \tag{9}$$

IV. Discussion of Results

The set of *tracked ageing parameters* was estimated for each cell and the results are summarised in Table II. Simulated voltages are matched well with measured voltages, with low root mean squared errors (RMSE), see Fig. 3. In case of the calendar aged cell, which experienced LLI, as expected, the stoichiometric limit on the anode decreased. Also, the kinetic rate constant decreased, suggesting an increase in resistance, most likely caused by SEI growth. The cycle aged cell experienced a decrease in active material volume fraction, corresponding to a loss of active material in the anode and a stoichiometric shift due to LLI. Diffusion time and kinetic overpotential both increased with cyclic ageing. The voltage prediction accuracy decreased in the cycle aged cell possibly due to cathode degradation which is not accounted for in the model. Nonetheless, model accuracy remained at an acceptable level. To highlight the importance of changing parameters during ageing, a model response using pristine reference parameters was simulated and compared to the cycled cell, and the RMSE increased to 178 mV.

The results of the heat balance simulations at 1C and C/3 using CC discharge for pristine and aged cells are shown in Fig. 4. Here reversible and irreversible heat contributions are compared. The calendar-aged group performance is nearly the same as the pristine group, even though the parameter optimisation revealed a decrease in k_-. The kinetic rate

Optimisation parameter	Pristine	Calendar aged	Cycle aged
x_-	0.74	0.7	0.7
x_+	0.26	0.27	0.35
$\varepsilon_{s,-}$	0.875	-	0.7
k_-	5.8e-11	4e-11	2.8e-11
λ_{D-}	1	-	0.7

TABLE II: Optimisation parameters results for groups pristine, calendar aged and cycle aged cells. The [-] denotes an unchanged value (reference value).

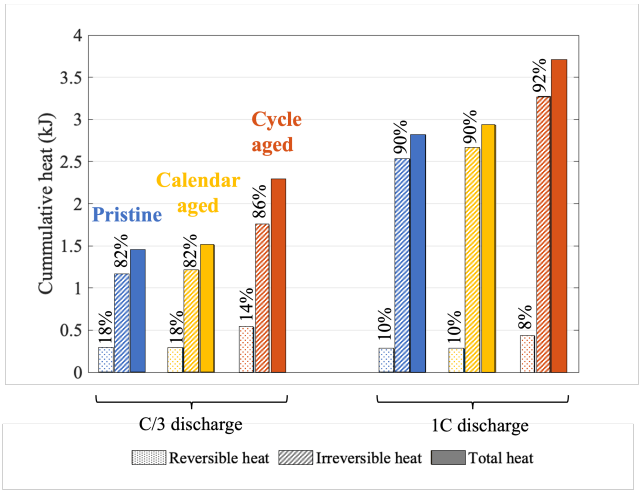

Fig. 4: Comparison of reversible and irreversible heat contributions during 1C and C/3 CC discharge from 100 % to 6 % SoC for pristine, calendar aged and cycle aged cells.

constant is directly linked to the irreversible heat generation, which is the main contributor of the total heat generation in discussed cells. The reversible heat in contrast contributes only 18% of total heat generation at C/3. The proportion of reversible heating decreases with C-rate increase.

Cycle-aged cells experienced ≈50% rise in irreversible heat generation during 1C discharge, demonstrating the significant impact of ageing on battery thermal performance. Changes in irreversible heating with cycle age are discussed in [3], and although (for discharge) the absolute value of the entropic heat increases with cyclic ageing, the irreversible heat rise is significantly higher, making the entropic contribution relatively smaller than in a pristine cell. The rise in irreversible heating is attributed to the significant decrease in k_-.

V. Conclusions

This work has presented a comparative study of the evolution of a subset of electrochemical parameters during ageing, comparing pristine, calendar-aged and cycled-aged Li-ion batteries. The goal was to investigate kinetic, transport and thermodynamic changes over battery lifetime via single particle model simulation and parameter optimisation. To avoid identifiability problems, only a specific subset of parameters was estimated in each case. The tracked parameters affected by ageing included the diffusion time, stoichiometry, active material volume fraction and kinetic rate constant. The main degradation mode revealed for the calendar-aged group was LLI, which resulted in a stoichiometric shift. This was accompanied by a decrease in kinetic rate, most likely caused by anode SEI growth. No significant changes in diffusion time for this group were noticed. There was a negligible change in the heat generation between pristine and calendar aged cell. On the other hand, the cycle-aged group experienced a decrease in the active material volume fraction, corresponding to LAM in the anode, and a stoichiometric shift due to LLI. Both diffusion time and kinetic overpotential increased with cyclic ageing. This was accompanied by ≈50% rise in irreversible heating.

In conclusion, the SPM voltage prediction accuracy can be maintained throughout battery lifetime within good limits ($15-32\,\mathrm{mV}$ RMSE) if certain model parameters are updated during ageing. However, this requires initial assumptions on what degradation modes/mechanisms are important, and in real applications they are often coupled. Although degradation on the anode was found to be prevalent for the data studied here, cathodic changes also happen which further complicates parameter identifiability.

References

[1] S. Wang, S. Jin, D. Deng, and C. Fernandez, "A critical review of online battery remaining useful lifetime prediction methods," *Front. Mech. Eng.*, vol. 7, pp. 719718–719737, 2021.

[2] S. G. Marquis, V. Sulzer, R. Timms, C. P. Please, and J. S. Chapman, "An asymptotic derivation of a single particle model with electrolyte," *J. Electrochem. Soc.*, vol. 166, no. 15, pp. A3693–A3706, 2019.

[3] M. E. Wojtala, A. A. Zülke, R. Burrell, M. Nagarathinam, G. Li, H. E. Hoster, D. A. Howey, and M. P. Mercer, "Entropy profiling for the diagnosis of NCA/Gr-SiO x Li-ion battery health," *ECSarXiv*, pp. 1–23, 2022.

[4] A. Zülke, Y. Li, P. Keil, R. Burrell, S. Belaisch, M. Nagarathinam, M. P. Mercer, and H. E. Hoster, "High-energy nickel-cobalt-aluminium oxide (NCA) cells on idle: anode- versus cathode-driven side reactions," *Batter. Supercaps*, vol. 4, pp. 1–15, 2021.

[5] J. Li, N. Lotfi, R. G. Landers, and J. Park, "A single particle model for lithium-ion batteries with electrolyte and stress-enhanced diffusion physics," *J. Electrochem. Soc.*, vol. 164, no. 4, pp. A874–A883, 2017.

[6] F. Brosa Planella, M. Sheikh, and W. D. Widanage, "Systematic derivation and validation of a reduced thermal-electrochemical model for lithium-ion batteries using asymptotic methods," *Electrochim. Acta*, vol. 388, pp. 138524–138548, 2021.

[7] A. Aitio, S. G. Marquis, P. Ascencio, and D. Howey, "Bayesian parameter estimation applied to the Li-ion battery single particle model with electrolyte dynamics," *arXiv*, pp. 1–8, 2020.

[8] S. Santhanagopalan, Q. Guo, and R. E. White, "Parameter estimation and model discrimination for a lithium-ion cell," *J. Electrochem. Soc.*, vol. 154, no. 3, pp. A198–A208, 2007.

[9] W. Plieth, *Electrochemistry for materials science*. Elsevier, 2008.

[10] C. Chen, F. Brosa Planella, K. O'Regan, D. Gastol, W. D. Widanage, and E. Kendrick, "Development of experimental techniques for parameterization of multi-scale lithium-ion battery models," *J. Electrochem. Soc.*, vol. 167, no. 8, pp. 080534–080557, 2020.

[11] L. Xia, E. Najafi, Z. Li, H. J. Bergveld, and M. C. F. Donkers, "A computationally efficient implementation of a full and reduced-order electrochemistry-based model for Li-ion batteries," *Appl. Energy*, vol. 208, no. May, pp. 1285–1296, 2017.

[12] E. Moyassari, T. Roth, S. Kücher, C. Chang, S. Hou, F. B. Spingler, and A. Jossen, "The role of silicon in silicon-graphite composite electrodes regarding specific capacity, cycle Stability, and expansion," *J. Electrochem. Soc.*, vol. 169, no. 1, pp. 010504–010516, 2022.

[13] E. Sarasketa-Zabala, F. Aguesse, I. Villarreal, L. M. Rodriguez-Martinez, C. M. López, and P. Kubiak, "Understanding lithium inventory loss and sudden performance fade in cylindrical cells during cycling with deep-discharge steps," *J. Phys. Chem*, vol. 119, no. 2, pp. 896–906, 2015.

[14] C. R. Birkl, M. R. Roberts, E. McTurk, P. G. Bruce, and D. A. Howey, "Degradation diagnostics for lithium ion cells," *J. Power Sources*, vol. 341, pp. 373–386, 2017.
[15] X. Li, A. M. Colclasure, D. P. Finegan, D. Ren, Y. Shi, X. Feng, L. Cao, Y. Yang, and K. Smith, "Degradation mechanisms of high capacity 18650 cells containing Si-graphite anode and nickel-rich NMC cathode," *Electrochim. Acta*, vol. 297, no. 303, pp. 1109–1120, 2019.
[16] S. J. Moura, N. A. Chaturvedi, and M. Krstić, "Adaptive partial differential equation observer for battery state-of-charge/state-of-health estimation via an electrochemical model," *J. Dyn. Syst. Meas. Control Trans. ASME*, vol. 136, no. 1, pp. 1–11, 2014.